E-shaped Aperture Coupled Microstrip Patch Array Antenna for High Speed Downlink Applications in Small Satellites

Kajol Chandra Paul, and Anis Ahmed

Abstract—**For high speed downlinking of payload data from small satellites, a new 4×4 aperture coupled microstrip patch array antenna has been presented. The antenna is designed for the Ku band and a peak gain of 18.0 dBi is achieved within the impedance bandwidth from 11.75 GHz to 12.75 GHz. Wide bandwidth is achieved as the patch elements are excited through E-shaped slots having asymmetric side lengths and widths. Each square patch element of the array with truncated corners and appropriately placed slots generates right hand circularly polarized (RHCP) radiation with very high cross-polarization discrimination. A corporate feed network consisting of T-junctions and quarter-wave impedance transformers is developed to feed the array elements from a single coaxial port of 50 Ω. To improve the radiation from the patches and wave-guiding in the feed network, two types of Rogers substrates with different dielectric constant and thickness are considered. Our proposed microstrip patch array antenna of size 7.8 cm × 6.4 cm × 0.3 cm can perform efficiently with a downlink data rate as high as 4.6 Gbps for small satellites.**

Keywords—**aperture coupled; circular polarization; corporate feed; microstrip patch array; small satellite**

I. INTRODUCTION

THERE have been increasing applications of the microstrip patch antenna in satellite communication for the last few decades, particularly in small satellites. It is useful to launch more small satellites such as minisat, microsat, nanosat, and picosat for the very essential radio relay and scientific data gathering purposes. For the Tracking, Telemetry, and Command (TT&C) subsystem, navigation (GNSS), payload, and inter-satellite communication, microstrip antennas are widely used. The launching cost of a satellite mainly depends on the mass and volume of the structure. A significant portion of the total weight and volume is covered by solar panels, batteries, on-board computers, transceiver, attitude determination and control system (ADCS), satellite framework, payload, etc. Besides, vibration and mechanical shock during the launch of a satellite, as well as the harsh space environment, play an important role in the antenna design. As a consequence, small satellite antennas need to be smaller, lighter, robust, and reliable.

Kajol Chandra Paul is with Dept. of Electrical and Electronic Engineering, Jatiya Kabi Kazi Nazrul Islam University, Mymensingh, Bangladesh (Correspondence e-mail: kajolc.paul@gmail.com).
Anis Ahmed is with Dept. of Electrical and Electronic Engineering, University of Dhaka, Dhaka, Bangladesh (e-mail: anis@du.ac.bd).

For TT&C and navigation purposes, a low gain antenna with a single patch can be enough. On the contrary, payload services need a high gain antenna for transmission of a large amount of data. As the small satellites in LEO orbit move very fast and remain visible for a brief period of time, a high data transmission rate is desirable to downlink more data in a shorter time. A coaxial-fed patch antenna in the S band providing 7.29-dBi gain has been proposed for payload data transmission in the HORYO-IV nanosatellite [1]. The researchers in [2] have presented a CPW-fed patch antenna for picosatellite, which has a gain of 7.3 dBi at 2.45 GHz. Several aperture-coupled patch antennas have been designed for CubeSat applications in the S band [3, 4]. Generally, aperture coupled antennas have better bandwidth characteristics than other feeding methods. To achieve sufficient wideband radiation for high speed data downlink, either the shape of the patch or the coupling slot should be modified [5]. Modification of slots is a more common process for bandwidth enhancement. Several types of slot configuration have been proposed in some literature, such as orthogonal cross-slots [6], ring-slots [7], inclined slots [8], E-shaped slots [9,10], etc. Few works are found where patch arrays have been constructed utilizing aperture coupled patch with E-shaped slots. Another important aspect of high speed data downlinking is to utilize higher frequency bands, for example, the X band [11] and the Ku band [12]. The authors in [13] have presented a meshed microstrip patch antenna at Ku band; 11.7-12.22 GHz downlink and 14.0-14.5 GHz uplink with 6.05-dBi and 7.61-dBi gain, respectively. Ku band downlink (10.7-12.7 GHz) and uplink (14-14.5 GHz) are utilized by TARS and GEN1 CubeSats for high-bandwidth data transfer [14]. These bands are significantly higher than the conventional frequency bands used for small satellites.

A single element microstrip patch can provide a maximum gain of 8 dBi [15], although that much gain is rarely achieved. Consequently, for higher gain, planar microstrip array antennas are preferred. A 2×2 patch array at 12 GHz operating frequency yielding a gain of 8.98 dBi has been reported in [16]. The authors in [17] have proposed two patch arrays, each having a gain of 12.4 dBi at 5.5 GHz. The arrays with a dimension of 23 cm × 10.5 cm are to be installed on the deployable wings of a CubeSat. A Fabry-Perot cavity antenna consisting of partially reflective surfaces of square patch

elements has been designed for small satellite applications in the X band with a gain of 14.7 dBi [18]. An X-band 4×4 patch array having a gain over 16 dBi has been designed by Endurosat [19]. Non-planar antennas are also utilized extensively in small satellites. A horn antenna achieving a gain of 15 dBi has been used in SSTL satellites [20]. Several types of deployable wire antennas, including dipole and log-periodic array, are investigated for CubeSat applications [21-23]. Deployable antennas need to be compactly stowed to the satellite chassis and then deployed once the satellite is in orbit. On the other hand, planar patch antennas can be comfortably integrated into the satellite structure, which makes them attractive for small satellites [24].

High gain antennas have narrow beamwidth. Small satellites often do not have high-precision beam pointing capability. Without such beam pointing, antennas with a medium gain of around 12 dBi can be used for data downlinking in small satellite [25]. Recently, there have been remarkable developments in ADCS for small satellites, in particular, a high-precision three-axis stabilization system has been incorporated in a nanosatellite [26]. These developments enable high-precision beam pointing and can pave the way for high-gain, narrow-beam antennas to be used for data downlink purposes.

In this paper, we propose a high gain and broadband circularly polarized microstrip patch array antenna to downlink small satellite payload data in the Gbps rate. The elements of the antenna are excited through asymmetric E-shaped apertures for obtaining wide bandwidth characteristics. This antenna is basically a five-layered structure having a total thickness of slightly less than 0.3 cm. The 4×4 flat-panel array has a compact size of 7.8 cm × 6.4 cm, which can be fitted on one side (presumably the earth-facing side) of a 1U CubeSat (10 cm × 10 cm × 10 cm). The antenna is designed at the center frequency of 12.2 GHz, and it exhibits a −10 dB impedance bandwidth of 1000 MHz. The array is powered with a single coaxial port. A corporate feeding network consisting of T-junctions and quarter-wave impedance transformers are employed for efficient power coupling. The antenna achieves a gain over 18.0 dBi throughout the impedance bandwidth. The patches are modified such that the array radiates right hand circularly polarized (RHCP) wave with an axial ratio (AR) of less than 3 dB.

The rest of the paper is assembled as follows. The design and the simulated results of the single-element patch are presented in section II. The extension of the single patch into a 4×4 array along with the design of feed network are discussed in Section III. An overall summary is given in Section IV.

II. SINGLE ELEMENT APERTURE COUPLED PATCH ANTENNA

A. Design of antenna geometry

As shown in Fig. 1(a), two different substrates are used for the patch and feed network. The top layer being the patch, the bottom layer is the feedline. The substrate material for the patch layer is Rogers RO3003 laminate with a dielectric constant, ϵ_{r1} of 3.00 and a thickness, h_p of 1.52 mm. The feed
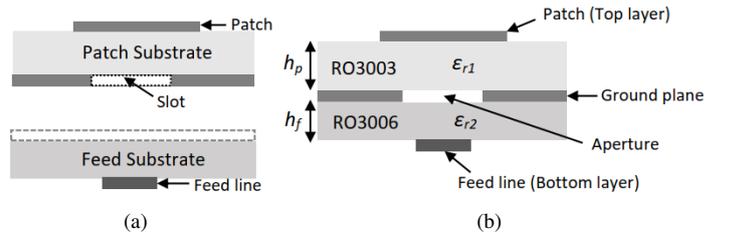

Fig. 1. (a) Patch and feed substrates are combined to create a five-layer aperture coupled patch antenna (the copper-clad on the top of the feed substrate is etched out, while the bottom side contains the feed line), and (b) The cross-sectional view of the aperture coupled five-layer single patch antenna.

substrate is Rogers RO3006 with dielectric constant, ϵ_{r2} of 6.15 and thickness, h_f of 1.28 mm. The thickness of the patch substrate is taken greater than that of the feed substrate, i.e., $h_p > h_f$, and that enables better radiation from the patches. To ensure better wave guiding between the feed structure and the ground plane, the dielectric constant of the feed substrate is taken larger than that of the patch substrate i.e., $\epsilon_{r2} > \epsilon_{r1}$. Both of the laminates have double-sided copper cladding, where RO3003 has 35 μm, and RO3006 has 17 μm thick copper foil. One side of the feed substrate is etched out, while the other side contains the feedline. For patch substrate, the copper cladding of one side acts as the common ground plane with a slot, while the other side houses the patch radiator. As aperture coupled feeding is used for the patch (Fig. 1(b)), the feed network and radiating patch element are isolated from each other. This helps to avoid leakage radiation from the feed line, and thus, cross-polarization and sidelobe levels (SLL) are greatly improved [27, 28].

The design of the proposed antenna is mainly focused on the new-age small satellite downlink operations in the lower Ku band from 11.7 GHz to 12.7 GHz. First, we shall present the design of a single element patch, which will be extended to construct an array of 4×4 elements. The geometrical configuration of the single element square patch is delineated in Fig. 2(a). The antenna is designed, analyzed, and optimised in CST Microwave Studio. For the design, the center frequency is chosen f_0 = 12.2 GHz, which corresponds to a free space wavelength, λ_0 = 24.57 mm. The optimized resonant length of the square patch is found, a = 5.88 mm.

Circular polarization (CP) is chosen for the proposed antenna as it ensures several key benefits over linear polarisation, especially for satellite communication. The CP signal is more immune to atmospheric factors, and there is no worry of misalignment with the transmitting and receiving antenna [29]. Many methods can be employed to generate circular polarization from a rectangular or square patch. Some of these methods use dual-fed patches, while others employ single feed. Dual-fed CP patches employ a hybrid branch line coupler or offset feed line that increases the overall size of the antenna and the complexity of the feed network in the array. Therefore, a single feed configuration is preferred over a dual feed. A singly-fed patch needs a perturbation region (which can be a slot or truncated segment) on the edge of the patch to create
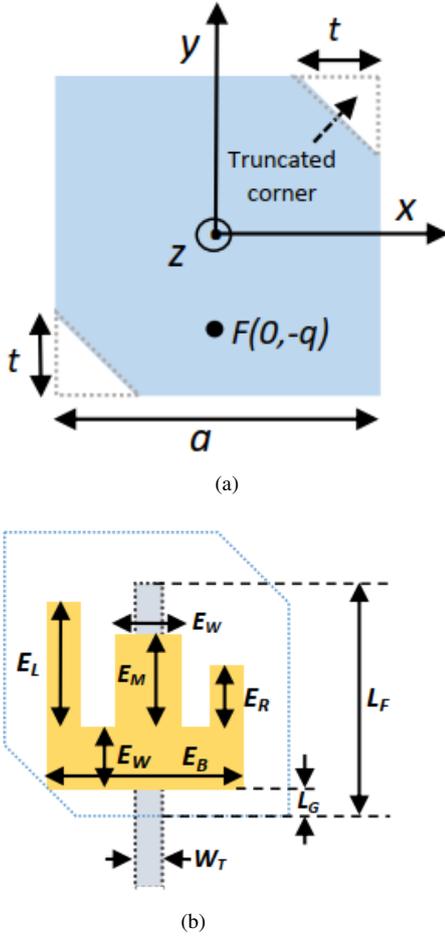
(a)

(b)

Fig. 2. (a) The structure of the square patch in which top right and the bottom left corners are stripped off to generate RHCP radiation, and (b) The E-shaped slot in the ground plane of the patch substrate with the feed line in the bottom layer of the feed substrate. The feed line is positioned right beneath the middle arm of the E-shaped slot for the excitation of the patch.

two orthogonally polarized modes. The location of the feeding point is also set in accordance with the perturbation region. To generate RHCP radiation, the top right and bottom left corners of the square patch need to be trimmed accurately, as shown in Fig. 2(a). The total perturbation area in the patch consisting of two chopped portions is approximately $\Delta S = t^2$. The length of the truncated corner, t can be found from the following equations [30].

$$\left(\frac{\Delta S}{S}\right)Q = \frac{1}{2} \tag{1}$$

$$t = \frac{a}{\sqrt{2Q}} \tag{2}$$

where S (= a^2) is the area of the unperturbed square patch and Q is the quality factor of the antenna. The value of Q can be calculated by [31, 32]

$$Q = \frac{VSWR - 1}{FBW\sqrt{VSWR}} \tag{3}$$

where FBW is the fractional bandwidth of the antenna where the VSWR is equal to or less than the desired value. Using Eqs. (1-2), the optimised value of t is found 1.86 mm.

The coupling amplitude for the aperture coupled patch can be determined as [33]

$$Coupling \simeq \sin\frac{\pi(a/2 - q)}{a} \tag{4}$$

where q is the distance along the y axis from the center of the patch. From Eq. (3), it follows that maximum coupling occurs when $q = 0$, i.e., the slot is placed at the center. To generate RHCP radiation, the location of the feeding point F is set in a way so that two orthogonal modes are excited with phase differences $+45°$ and $-45°$ with respect to the feed point [21]. As shown in Fig. 2(a), the feed is placed at an offset location, $F(0, -q)$ from the center such that $|q| \leq a/2$. In our design, the optimum position of the slot is found near the bottom edge of the patch ($q \approx a/2$) to produce CP radiation in the boresight direction. To be exact, the slot is placed at $L_G =$ 0.85 mm from the bottom edge of the patch. Referring to Fig. 2(b), the length of the microstrip feed line below the patch is optimized to get $L_F = 3.85$ mm. The feed line has a width, $W_T = 0.36$ mm and an impedance of 100 Ω. The impedance of a patch is maximum at the edge and decreases towards the center. Thus, the location of the slot determines the impedance. In particular, the length (L_F) and width (W_T) of the feed line is critical to attain impedance matching with respect to the location of the slot below the patch.

TABLE I
OPTIMIZED DESIGN PARAMETERS OF THE ELEMENT PATCH

Parameter	Value (mm)	Parameter	Value (mm)
a	5.88	E_B	3.75
t	1.86	E_L	1.57
L_F	3.85	E_M	1.25
L_G	0.85	E_R	0.90
W_T	0.36	E_W	1.00

As shown in Fig. 2(b), the E-shape aperture has three vertical arms with asymmetric lengths and widths. The lengths of the left, middle, and right arms are defined, respectively, as E_L, E_M, and E_R, while the base of the shape E has length E_B and width E_W. The width of the middle arm is same as the base width. These parameters along with a and t are properly adjusted so that the resonance frequency of the patch is split into two resonant modes and a broad impedance bandwidth is obtained. The optimized dimensions for the single element patch antenna are given in Table I.

B. Simulated results of the antenna

The S_{11} and VSWR of the single element patch are shown in Fig. 3. As illustrated in the figure, the single element patch has a -10 dB impedance bandwidth of 22.1% or 2700
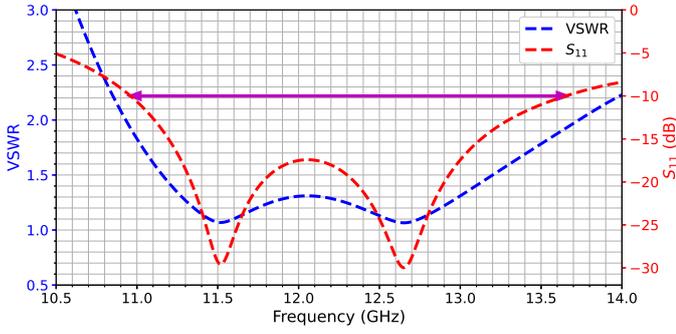
Fig. 3. The S_{11} and VSWR of the single patch antenna. The double-headed horizontal arrow indicates the operating bandwidth from 10.96 GHz to 13.66 GHz for $S_{11} < -10$ dB.

MHz, ranging from 10.96 GHz to 13.66 GHz. The impedance bandwidth is indicated by the double-headed horizontal arrow in the figure. The broad bandwidth is achieved as the resonance frequency is split in two frequencies (f_1 = 11.52 GHz and f_2 = 12.65 GHz) by optimizing the parameters such as E_L, E_M, E_R, E_B, a, and t. Changing these values directly affects f_1 and f_2, and the bandwidth. For example, if the value of t is decresed, f_1 and f_2 comes closer, decreasing the overall bandwidth. On the other hand, increasing t set the frequencies far apart, decreasing the S_{11} and AR values. The VSWR value is found less than 2 throughout the impedance bandwidth.

The antenna has a broadside radiation pattern, as is illustrated in Fig. 4. The values are given with respect to angle θ for two constant ϕ angles. Referring to Fig. 2, angle θ is measured from the z axis to the xy plane (i.e., antenna plane), while angle ϕ is measured from the x axis to the y axis. It can be observed that the designed antenna provide RHCP radiation with low level of cross-polarization at boresight. This indicates that an excellent level of polarization purity is achieved. Peak level of cross-polarization discrimination is achieved at the center frequency 12.2 GHz. The single element patch antenna has a peak gain of 6.95 dBi along $\theta = -3°$ and a half power beamwidth (HPBW) of 90.4° and 75.3°along $\phi = 0°$ and $\phi = 90°$ plane, respectively.

Figure 5 shows the contour plots of the electric field distribution with respect to phase angles 0°/360°, 90°, 180°,

Fig. 5. Contour plot of the electric field component normal to the antenna plane for various phase angles. This 2D graphical plot illustrates the clockwise rotation (source point of view) of the electric field component and confirms the RHCP radiation.

and 270°. As seen from the top of the page, the normal component of the electric field attributes an anticlockwise rotation due to the fact that the patch is right hand circularly polarized. From the point of view of the source, the electric field component rotates clockwise in a plane perpendicular to the direction of propagation.

C. Farfield projection from single patch to array

Antenna gain can be substantially increased by making an array of many patch elements. In arrays, doubling the number of patch elements doesn't double the gain. It was observed that a 3-dB increase in directivity is achieved each time microstrip apertures are doubled [34]. Figure 6 is found by far-field approximation using CST software. It predicts the radiation pattern if the single patch is extended to an array of multiple elements. It is observed that, if the number of elements in an
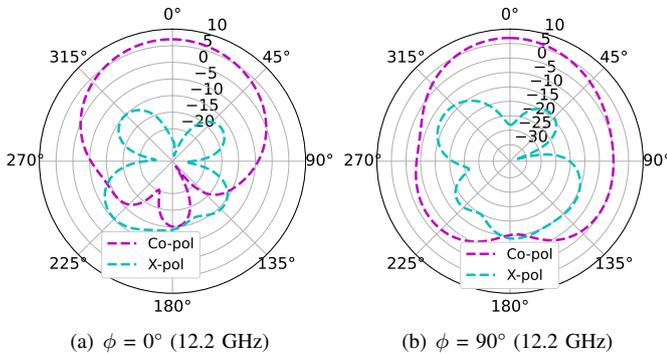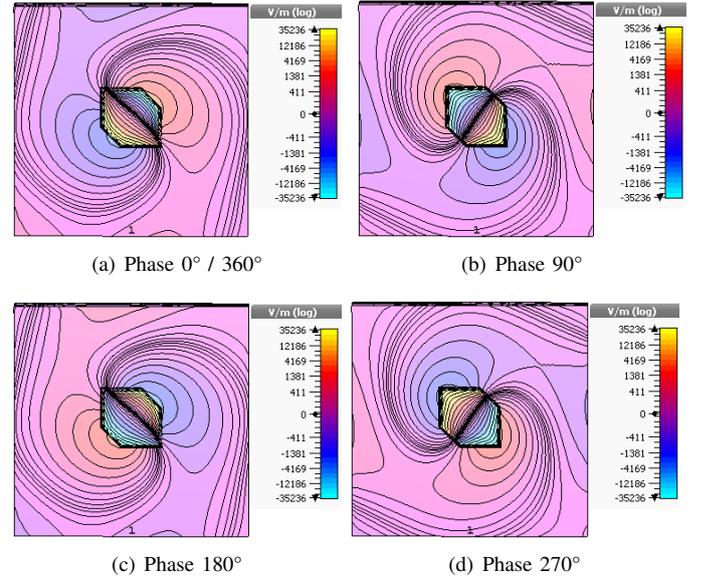

Fig. 4. The polar radiation pattern for the right hand (Co-pol) and left hand (X-pol) circular polarization at 12.2 GHz along the $\phi = 0°$ and $\phi = 90°$ orthogonal cut-planes.
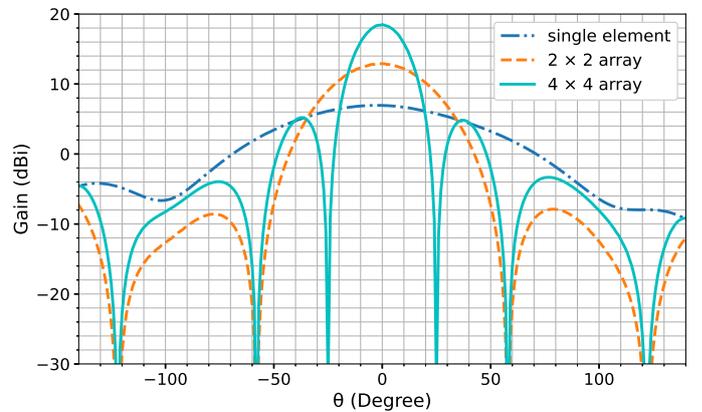

Fig. 6. Farfield projection performed in CST software predicts the gain pattern if the single element patch is extended to arrays of 2×2 and 4×4 elements.

array increases, the gain of the antenna also increases while the radiation beam gets narrower. The gain is projected around 13 dBi when the single patch is extended to an array of 2×2 elements. If it is further extended to 4×4 elements array, a narrow radiation pattern with a gain of over 18 dBi can be found. In the next section, the design of the 4×4 elements array is described in detail.

III. 4×4 APERTURE COUPLED PATCH ARRAY ANTENNA

To achieve narrow beam radiation with high values of gain for high speed data downlink, the single element patch is extended to an array of 4×4 or 16 elements. The main challenge is to develop the feeding network for the excitation of the patches from a single coaxial port. In Section II, we have presented the design to determine the parameters related to the E-shaped slot, and the patch element. But in designing the array of 4×4 elements, the characteristics of the element patch such as the return loss, radiation pattern, axial ratio, etc., are partly affected due to the mutual coupling between neighbouring elements and unwanted radiation from the feed network. Consequently, the array antenna is optimized with regard to patch-dimension, truncated corner length, inter-element spacing, and the parameters associated with the E-shape slot to obtain the desired characteristics.

A. Array structure

The two dimensional array geometry along with the E-shaped coupling slots and feed network is shown in Fig. 7. The inter-element spacing (patch edge-to-edge) is denoted by d (d_x for element separation in the x-direction and d_y for element separation in the y-direction). The size of the array can be approximately defined as $4a + 3d + 2X$, where the length and width of the antenna panel are respectively, $L = 4a + 3d_x + 2X$ and $W = 4a + 3d_y + 2X$. Here, X denotes the extra space from the outer patch edge to substrate edge on both sides,

and $X \approx a$. To avoid any grating lobes, d must be less than one wavelength, that is, $d < \lambda_0$. Further, to constrain the size of the array below a 1U CubeSat (< 100 mm), d is chosen even smaller. However, the effect of mutual coupling is more pronounced at smaller d. Thus, a trade-off is made for the inter-element spacing, and we have chosen $d_x = 0.59\lambda_0$, $d_y = 0.40\lambda_0$ to get a better radiation characteristics. Varying the inter-element spacing in the x and y axis helps to tailor the beamwidth along $\phi = 0°$ and $\phi = 90°$ plane. With the optimized patch-dimension $a = 5.60$ mm, the size of our proposed array antenna becomes 7.8 cm × 6.4 cm, which can be mounted on a 1U CubeSat easily.

B. Feed network design

A corporate feed network is employed for the excitation of the elements of the array, as illustrated in Fig. 7. The antenna is powered with a single SMA coaxial port having an impedance of 50 Ω. The main feedline of the array having a width, W_{FA} connects the coaxial port to the rest of the network. The impedance of the main feedline $Z_{W_{FA}}$ is also taken 50 Ω to ensure impedance matching. After the port is energized, the signal power is progressively divided through power-splitting T-junctions.

In total, there are 15 T-junctions, numbered **1** through **15** in the figure. Junction **1** is a simple T-junction, while the rest of the junctions from **2** to **15** are quarter-wave matched T-junctions. The quarter-wave matched T-junctions incorporate quarter-wave impedance transformers (QWIT) to reduce standing waves in the feed line. In the outermost T-junctions, from **8** to **15**, one of the output arms is a microstrip stub, M_S while the other arm, M_B contains mitered bends. M_S and M_B can be of the same or different electrical lengths depending on the phase relationship of the two signals they carry. Creating a small phase difference between them, the antenna beam can be steered along the y axis. M_B uses mitered bends so that a path difference or phase difference can be created between the patch elements along the y axis without altering d_y. The input and output line impedances of the simple T-junction (**1**) are related by

$$Z_{W_T} = 2\,Z_{W_F} \tag{5}$$

where Z_{W_T} corresponds to the impedances of the output arms of the simple T-junction, and $Z_{W_T} = 100$ Ω. Two output arms of the junction have equal width (i.e., W_T) and hence equal impedance (i.e., Z_{W_T}). So, equal power division occurs here. Similarly, all the output arms of the quarter-wave matched T-junctions (**2** to **15**) have width, W_T, and impedance, $Z_{W_T} = 100$ Ω. The quarter-wave matching transformers (i.e., QWIT) have length, L_M, and width, W_M. To match the impedances, the length, L_M is made equal to the quarter of the free space wavelength, i.e., $L_M = \lambda_0/4$. The impedance of the quarter-wave matching transformer, Z_{W_M} is found as [35]

$$Z_{W_M} = Z_{W_T}/\sqrt{2} \tag{6}$$

The thickness and dielectric constants of the substrates determine the size of the feed lines and power division
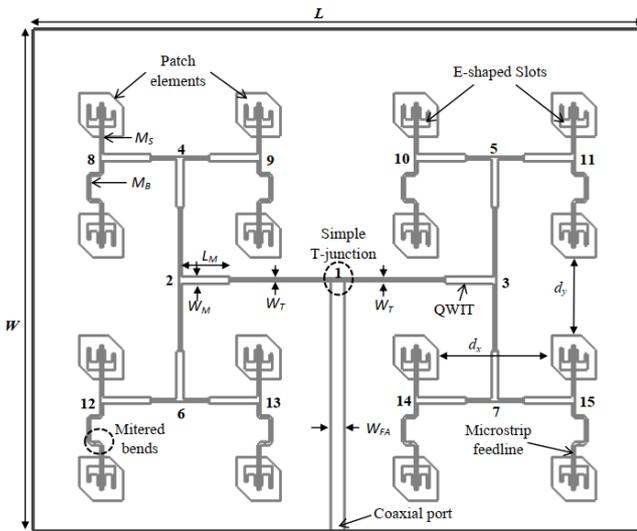

Fig. 7. The corporate feed network at the bottom layer of the antenna consists of power-splitting T-junctions and mitered bends. The slots on the ground plane and the patch elements in the top layer are also shown.

TABLE II
FEEDLINE WIDTH AND CORRESPONDING IMPEDANCE

Feedline width (mm)		Impedance (Ohm)	
W_{FA}	1.75	$Z_{W_{FA}}$	50
W_T	0.36	Z_{W_T}	100
W_M	0.90	Z_{W_M}	70.71

network. The widths of microstrip lines in the feed network are calculated based on their corresponding impedances and the values are shown in Table II. The feed network in the bottom layer ensures smooth power flow without incurring much reflection losses and thus, excites the patch elements in the top layer.

C. Simulated results of the array

1) S_{11} characteristics: As discussed previously, the design parameters of the single patch are optimized further to achieve the desired characteristics of the array antenna. For the convenience in analysis, let us consider three cases: *Case-A*, *Case-B*, and *Case-C* (Table III). Figure 8 depicts the S_{11} characteristics for the three cases. *Case-A* describes the optimized parameters which exhibit the best results for the array antenna. *Case-B* and *Case-C* describe two circumstances where some parameters are changed back to the single element optimized values, keeping other parameters constant. *Case-B* considers the state where only a and t are changed to 5.88 and 1.86, keeping the remaining parameters constant. In *Case-C*, the three arms of the shape-E slots in array are set to the same values as in case of single element i.e., $E_L = 1.57$, $E_M = 1.25$, $E_R = 0.90$. For $Case_A$, a broad impedance bandwidth of 1000 MHz, ranging from 11.75 GHz to 12.75 GHz is found. It is clearly seen from the figure that the best result is obtained for the parameters as specified for *Case-A* in Table III. The impedance bandwidth of the array shrinks by 63% from that of the single element patch, shown in Fig. 3. The decrease of impedance bandwidth of the array may be due to the increase in gain from the single patch-element to the 16 elements array. In the two other cases, the bandwidth decreases from that of the $Case_A$. It is also evident that, the single element characteristics change when it is extended to an array, requiring new optimization to obtain the desired features. The new optimized dimensions in the array are given in Table III.

2) Gain and axial ratio: The maximum gain, as well as the axial ratio is presented in Fig. 9. It is observed that the maximum gain achieved is 18.3 dBi while the antenna maintains a gain of over 18 dBi within the impedance bandwidth. On the other hand, the AR curve shows that, at 12.2 GHz, the AR value is the lowest i.e., 0.43 dB. The 3-dB AR bandwidth is from 12.03 GHz to 12.48 GHz, that estimates to 450 MHz. The AR bandwidth is generally smaller than the impedance bandwidth in single feed CP antennas.

3) VSWR and efficiency: A highly efficient antenna will radiate most of the power it receives. As shown in Fig. 10,
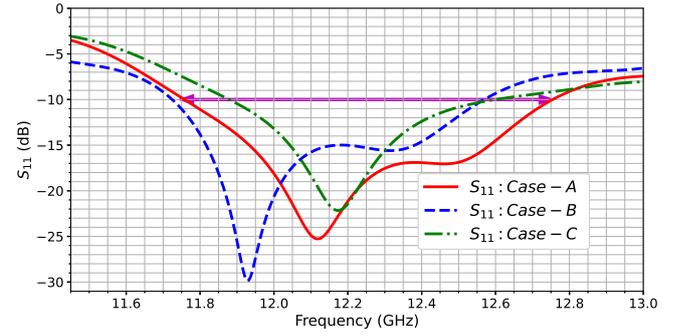

Fig. 8. S_{11} characteristics of the array anteena. An impedance bandwidth of 1000 MHz or 8.2 % is achieved with the new optimized values.
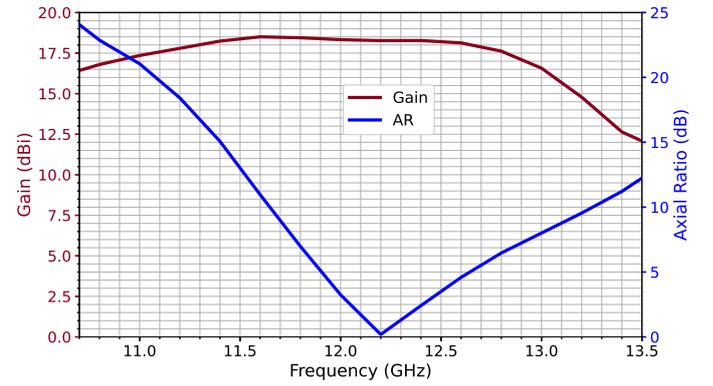

Fig. 9. The maximum gain and axial ratio (AR) over frequency. The antenna maintains a gain of over 18.0 dBi throughout the impedance bandwidth. It also exhibits a good axial ratio (<3 dB) from 12.03 GHz to 12.48 GHz.

the VSWR value is 1.2 at the center frequency. The radiation efficiency of the antenna is 85.6%, while the total efficiency is 85.0%. The total efficiency of the antenna considers the losses due to impedance mismatch and conductive and dielectric losses in the antenna. Hence, it is evident from the figure that an adequate impedance matching has been achieved.

TABLE III
OPTIMIZED DESIGN PARAMETERS OF THE ARRAY

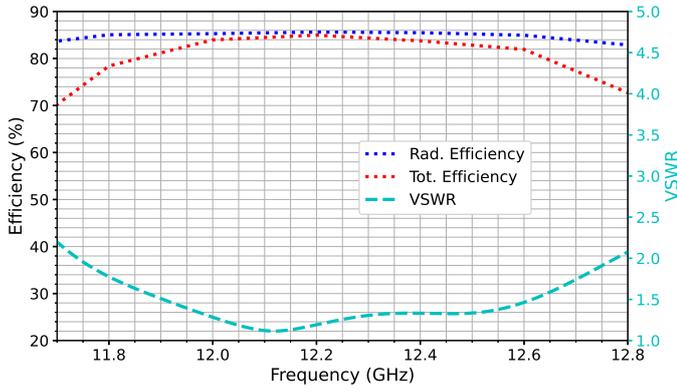| Parameter	Value (mm)		
	Case-A	*Case-B*	*Case-C*
a	**5.60**	**5.88**	5.60
t	**1.77**	**1.86**	1.77
E_L	**1.80**	1.80	**1.57**
E_M	**1.50**	1.50	**1.25**
E_R	**1.00**	1.00	**0.90**
L_F	**4.30**	4.30	4.30
E_B	**3.50**	3.50	3.50
L_G	**1.20**	1.20	1.20

Fig. 10. Total efficiency, Radiation efficiency, and VSWR of the antenna with respect to frequency. It's a low loss antenna having both efficiencies at greater than 85%.

4) Radiation pattern: Fig. 11 shows the 3D plot of the array farfield radiation where the gain of the major lobe is 18.3 dBi. The gains of the sibe lobes are significantly lower than the main lobe. The corporate feed network used in the array has 15 junctions and 32 bends which can generate undesired radiation and increase the sidelobe [34]. Using the aperture coupling method is beneficial as it shields the undesired radiation from the feed network. Thus, the radiations from the individual patches are unaffected. Consequently, the array gives rise to a radiation beam with high gain and low sidelobes.

Figure 12 shows the antenna farfield gain pattern and axial ratio. Both the gain and the axial ratio are shown with respect to θ angles for two orthogonal cut-planes, i.e., $\phi = 0°$ and $\phi = 90°$. The main lobe direction is at $\theta = 0°$, indicating the broadside radiation pattern of the antenna. The half power beamwidth (HPBW) is 15.0° and 19.9° along $\phi = 0°$ and $\phi = 90°$ plane, respectively. The SLL is -12.0 dB and -10.4 dB in the respective planes. In Fig. 12(a), the angular width along θ, enclosed by two vertical lines, shows the corresponding HPBW. Larger inter-element spacing in the x axis results in narrower beamwidth in the $\phi = 0°$ plane. As illustrated in Fig. 12(b), axial ratio is less than 3 dB throughout the entire HPBW, which signifies a CP wave in the main lobe.

5) Cross polarization isolation: Mutual coupling between the radiating elements in a circularly polarized array can deteriorate radiation characteristics, especially the polarization characteristics. Figure 13 illustrates polarization pattern along $\phi = 0°$ plane and $\phi = 90°$ plane. As shown in the figure, the array generates a nearly pure RHCP beam with very high cross-pol isolation (i.e., low cross-polarization) in the

(a) Gain at $\phi = 0°$ and $\phi = 90°$.

(b) Axial ratio at $\phi = 0°$ and $\phi = 90°$.

Fig. 12. Cartesian plot of (a) Gain and (b) axial ratio at $\phi = 0°$ and $\phi = 90°$ plane with respect to θ. HPBW is greater along $\phi = 0°$ plane. AR is less than 3 dB throughout the HPBW.
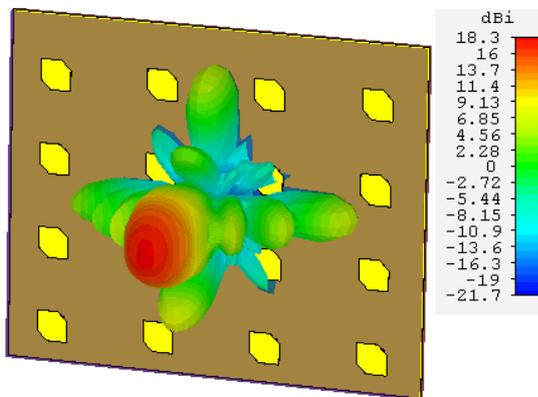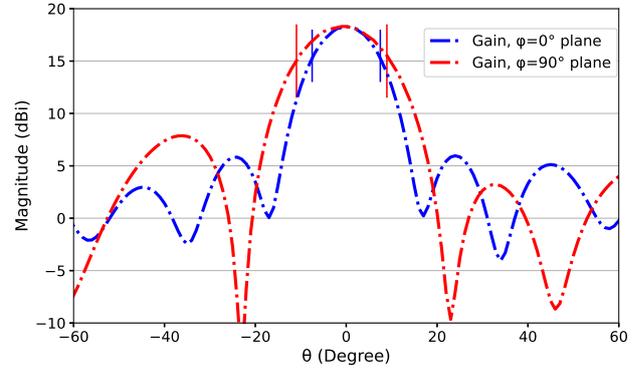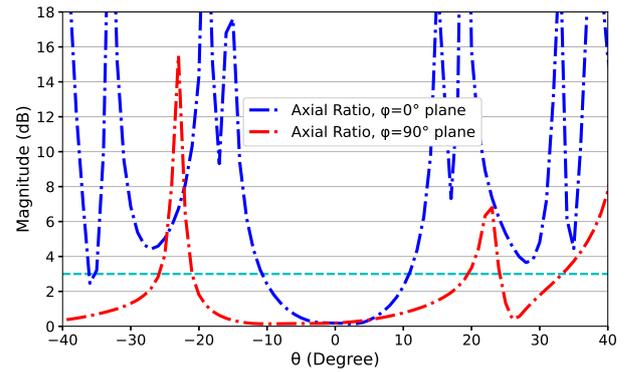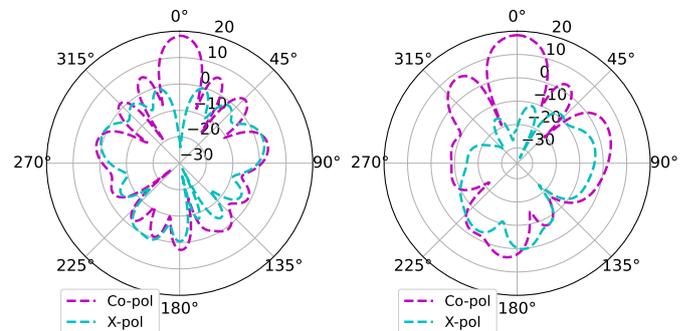

Fig. 11. 3D farfield plot of the array. It has a narrow beam concentrated at the centre of the structure and the side lobes are greatly reduced.

(a) Polarization pattern along $\phi = 0°$ (b) Polarization pattern along $\phi = 90°$

Fig. 13. The RHCP and LHCP pattern along (a) $\phi = 0°$ plane and (b) $\phi = 90°$ plane for $d_x = 0.59\lambda_0$, $d_y = 0.40\lambda_0$. A very low level of cross polarization is achieved in the boresight direction.

boresight direction for $d_x = 0.59\lambda_0$ and $d_y = 0.40\lambda_0$. In both planes, the level of cross polarization isolation achieved exceeds 30 dB. If the values of d_x and d_y are decreased, mutual coupling between the patch elements becomes prominent. As a result, the main lobe shifts and nulls appear close to the broadside direction. Moreover, the cross-polarization is significantly increased. On the other hand, if the values of d_x and d_y are substantially increased, grating lobes appear which results in poor SLL wasting power in undesired directions. Thus, we have taken $d_x = 0.59\lambda_0$ and $d_y = 0.40\lambda_0$, which is also used for calculation of total array-size.

TABLE IV
PERFORMANCE COMPARISON OF THE SINGLE ELEMENT AND THE 4×4 ELEMENTS ARRAY ANTENNA

Characteristics	Single Element Patch Antenna	4×4 Elements Array Antenna
Elements	1	16
f_0 (GHz)	12.2	12.2
OFR* (GHz)	10.96-13.66	11.75-12.75
BW (MHz)	2700 (22.1%)	1000 (8.2%)
Polarization	RHCP	RHCP
η (%)	94.8	85.6
AR at f_0	0.55	0.43
HPBW ($\phi = 0°, 90°$)	90.4°, 75.3°	15.0°, 19.9°
Gain (dBi)	6.95	18.0
Grating lobes	No	No
SLL (dB)	−11.1	−12.0
Size (cm^2)	2.0 × 2.5	7.8 × 6.4

* Operating frequency range

The important characteristics of the designed 4×4 aperture coupled array as well as the single element antenna are summarized in Table IV. As can be noticed from the table, a high-gain, narrow-beam, broadband CP radiation is found from the array at the expense of a bigger antenna size.

D. Calculation of downlink data rate of the array

Let us suppose that the proposed array antenna is mounted on a CubeSat to transmit (downlink) the payload data to the ground stations. The bandwidth (1000 MHz) and gain (18.0 dBi) of the array antenna are denoted by B and G_T, respectively. The data rate or throughput can be calculated from Shannon channel capacity formula using channel bandwidth and Signal to Noise Ratio (SNR)

$$CC = B \log_2 (1 + SNR) \qquad (7)$$

where CC is the channel capacity (i.e., data rate) in bits per second (bps), and SNR is the signal to noise ratio at the receiving station. Employing the satellite downlink budget equations described in [36-38], the SNR is calculated for a CubeSat assuming a transmit power, P_T of 2 W. The distance, D between the ground station and satellite is assumed 1000 km. Let the receiving antenna gain, G_R at the ground station

TABLE V
DETERMINATION OF CHANNEL CAPACITY THROUGH DOWNLINK BUDGET ANALYSIS

Attributes	Magnitude	Attributes	Magnitude
f_r	12.2 GHz	T	290 K
B	1000 MHz	$[P_N]$	−153.9 dB
$[P_T]$	3 dBW	$[G_R]$	30 dBi
$[G_T]$	18.0 dBi	$[LL]$	3.5 dB
$[EIRP]$	21.0 dBW	$[SNR]$	27.2 dB
D	1000 Km	SNR	22.9
$[FSPL]$	174.2 dB	CC	4.6 Gbps
K	1.38×10^{-27}		

be 30 dBi for a typical parabolic reflector type antenna. The equivalent isotropic radiated power ($EIRP$) is found as

$$[EIRP] = [P_T] + [G_T] \, dBW \qquad (8)$$

where $[P_T]$ is in dBW and $[G_T]$ is in dBi (For clarity, the Parameters in decibel are enclosed by square brackets). The free space path loss ($FSPL$) can be calculated from the following formula

$$[FSPL] = 92.45 + 20 \log D + 20 \log f_r \qquad (9)$$

where D is in km and f_r is in GHz. The noise power, P_N is calculated as

$$[P_N] = 10 \log (KTB) \, dB \qquad (10)$$

where K is the Boltzmann's constant, and T is the equivalent noise temperature at the receiver.

The SNR of the downlink signal (from satellite to the ground station) can be estimated in dB with the following equation

$$[SNR] = [EIRP] + [G_R] - [P_N] - [FSPL] - [LL] \qquad (11)$$

where LL denotes link losses, which include atmospheric loss, rain attenuation, antenna misalignment loss, etc. Considering $T = 290$ K and $LL = 3.5$ dB, the calculations are performed and the obtained results are presented in Table V. It is observed that a data rate as high as 4.6 Gbps can be achieved for payload data downlinking. It follows that our proposed model has achieved a higher gain, and higher bandwidth at a comparatively lower size. This demonstrates that the antenna can potentially be used as a high speed downlink antenna in small satellites, especially CubeSats.

IV. CONCLUSION

A 4×4 elements aperture coupled circularly polarized microstrip array antenna has been presented for small satellite payload data downlinking at Ku band. Antenna characteristics are analyzed and optimized in CST Microwave Studio. Asymmetric E-shape slots are used to obtain broad impedance bandwidth of 1000 MHz, from 11.75 GHz to 12.75 GHz.

The array exploits an efficient corporate feeding network to excite the truncated-corner square patch elements. A peak gain of over 18.0 dBi has been achieved over the impedance bandwidth. The axial ratio below 3 dB is from 12.03 GHz to 12.48 GHz, corresponding to an AR bandwidth of 450 MHz. The maximum dimension of the array panel measures only 7.8 cm, which is less than the dimension of a 1U CubeSat. The simulated results exhibit that the proposed model can be used for high speed payload data downlinking in small satellites.

REFERENCES

[1] M. T. Islam, M. Cho, M. Samsuzzaman, and S. Kibria, "Compact Antenna for Small Satellite Applications", *IEEE Antennas and Propagation Magazine*, 57 (2), pp. 30-36 (2015), https://doi.org/10.1109/MAP.2015.2420471.

[2] F. E. Tubbal, R. Raad, and K. Chin, "A Survey and Study of Planar Antennas for Pico-Satellites", *IEEE Access*, 3, pp. 2590-2612 (2015), https://doi.org/10.1109/ACCESS.2015.2506577.

[3] T.R. Jones, J.P. Grey, and M. Daneshmand, "Solar Panel Integrated Circular polarized Aperture-Coupled Patch Antenna for CubeSat Applications", *IEEE Antennas and Wireless Propagation Letters*, 17(10), pp. 1895-1899 (2018), https://doi.org/10.1109/LAWP.2018.2869321.

[4] M. J. Veljovic, and A. K. Skrivervik, "Aperture-Coupled Low-Profile Wideband Patch Antennas for CubeSat", *IEEE Transactions on Antennas and Propagation*, 67(5), pp. 3439-3444 (2019), https://doi.org/10.1109/TAP.2019.2900428.

[5] G. Kumar and K. P. Ray, "Broadband Microstrip Antennas" (Artech House Inc., London, UK, 2003, 1st edn.), pp. 331–353.

[6] M. A. B. Kortright and R. N. Simons, "K-Band Cross-Aperture Coupled Circularly Polarized Dual Frequency Microstrip Patch Antenna with Single Feed," *2018 IEEE International Symposium on Antennas and Propagation & USNC/URSI National Radio Science Meeting*, Boston, MA, USA, pp. 337-338, July 2018, https://doi.org/10.1109/APUSNCURSINRSM.2018.8608618.

[7] C. H. Lai, T. Y. Han, and T. R. Chen, "Broadband aperture-coupled microstrip antennas with low cross polarization and back radiation," *Progress In Electromagnetics Research Letters*, 5, pp. 187-197 (2008), https://doi.org/10.2528/PIERL08111805.

[8] K. P. Yang, and K. L. Wong, "Inclined-slot-coupled compact dual-frequency microstrip antenna with cross-slot," *Electronics Letters*, 34(4), pp. 321-322 (1998). https://doi.org/10.1049/el:19980222.

[9] X. F. Zhu and D. L. Su, "Symmetric E-shaped slot for UWB antenna with band-notched characteristic," *Microwave and Optical Technology Letters*, 52 (7), pp. 1594–1597 (2010), https://doi.org/10.1002/mop.25284.

[10] A. Dastranj and H. Abiri, "Bandwidth Enhancement of Printed E-Shaped Slot Antennas Fed by CPW and Microstrip Line," *IEEE Transactions on Antennas and Propagation*, 58 (4), pp. 1402-1407 (2010), doi: https://doi.org/10.1109/TAP.2010.2041164.

[11] S. Chen, and M. Shie, "A Compact High Gain X-Band Patch Antenna for Cube and Small Satellite Applications", *IEEE International Symposium on Antennas and Propagation and USNC-URSI Radio Science Meeting*, Atlanta, GA, USA, pp. 1561-1562, July 2019, doi: https://doi.org/10.1109/APUSNCURSINRSM.2019.8888759.

[12] M. Samsuzzaman, M. T. Islam, N. Misran, and M. A. Mohd Ali, "Dual Band X Shape Microstrip Patch Antenna for Satellite Applications", *Procedia Technology*, 11, pp. 1223-1228 (2013), https://doi.org/10.1016/j.protcy.2013.12.317.

[13] F. Nashad, S. Foti, D. Smith, M. Elsdon, and O. Yurduseven, "Ku-band suspended meshed patch antenna integrated with solar cells for remote area applications", *Progress In Electromagnetics Research*, 83, pp. 245-254 (2018), https://doi.org/10.2528/PIERC18020608.

[14] "A Network to Connect the Globe," https://www.keplercommunications.com/network#tars-slide, accessed December 2020.

[15] R. B. Waterhouse, "Microstrip Patch Antennas: A Designer's Guide" (Springer Science+ Business Media, New York, USA, 2003, 1st edn.), pp. 327-350.

[16] T. T. S. Borel, A. R. Yadav, and U. Shah, "Design of Rectangular Patch Array Antenna for Satellite Communication", *3rd International Conference on Computing Methodologies and Communication (ICCMC)*, Erode, India, pp. 759-764, March 2019, https://doi.org/10.1109/ICCMC.2019.8819861.

[17] P. Bouca, J. N. Matos, S. Cunha, and N. B. Carvalho, "Low-Profile Aperture-Coupled Patch Antenna Array for CubeSat Applications," *IEEE Access*, 8, pp. 20473–20479 (2020), https://doi.org/10.1109/ACCESS.2020.2968060.

[18] F. Qin, S. Gao, G. Wei, Q. Luo, C. Mao, C. Gu, J. Xu, and J. Li, "Wideband Circularly polarized Fabry-Perot Antenna", *IEEE Antennas and Propagation Magazine*, 57(5), pp. 127-135 (2015), https://doi.org/10.1109/MAP.2015.2470678.

[19] "X-Band 16 Element Patch Antenna Array," https://satcatalog.com/component/x-band-4x4-patch-antenna/, accessed January 2021.

[20] "Satellite Platforms," https://www.sstl.co.uk/what-we-do/satellite-platforms, accessed January 2021.

[21] C. E. Lesanu and A. Done, "Parasitic circular polarized vertical antennas," *International Conference on Development and Application Systems (DAS)*, Suceava, Romania, pp. 143-149, May 2016, https://doi.org/10.1109/DAAS.2016.7492564.

[22] A. T. Joseph, M. Deshpande, P. E. O'Neill, and L. Miles, "Development of VHF (240–270 MHz) antennas for SoOp (signal of opportunity) receiver for 6U Cubesat platforms," *Progress in Electromagnetic Research Symposium (PIERS)*, Shanghai, China, pp. 2530-2531, August 2016, https://doi.org/10.1109/PIERS.2016.7735037.

[23] J. Costantine, Y. Tawk, A. Ernest, and C. G. Christodoulou, "Deployable antennas for CubeSat and space communications," *6th European Conference on Antennas and Propagation (EUCAP)*, Prague, Czech Republic, pp. 837-840, March 2012, https://doi.org/10.1109/EuCAP.2012.6206124.

[24] S. Gao, Y. Rahmat-Samii, R. E. Hodges, and X. X. Yang, "Advanced Antennas for Small Satellites," *Proceedings of the IEEE*, 106(3), pp. 391-403 (2018), https://doi.org/10.1109/JPROC.2018.2804664.

[25] K. Devaraj, "Small Satellite Antennas," in Pelton, J.N., Madry, S. (Ed.): "Handbook of Small Satellites" (Springer, Chapel Hill, NC, USA, 1st edn.), pp. 203-213 (2020).

[26] "CanX-2: System Overview," https://www.utias-sfl.net/?page_id=172, accessed February 2021.

[27] J. Huang, "Microstrip Antennas: Analysis, Design, and Application," in Balanis, C. A. (Ed.): "Modern Antenna Handbook" (John Wiley & Sons Inc., USA, 2008, 1st edn.), pp. 157–196.

[28] C. A. Balanis, "Antenna Theory - Analysis and Design," (John Wiley and Sons Ltd., New York, NY, USA, 2005, 3rd edn.), pp. 811–872.

[29] "Circular polarisation vs. Linear polarisation-Intelsat," http://www.intelsat.com/wp-content/uploads/2013/02/polarisation.pdf, accessed February 2021.

[30] M. Haneishi and S. Yoshida, "A design method of circularly polarized rectangular microstrip antenna by one-point feed," *Electronics and Communications in Japan (Part I: Communications)*, 64 (4), pp. 46–54 (1981), https://doi.org/10.1002/ecja.4410640407.

[31] K. Carver and J. Mink, "Microstrip antenna technology," *IEEE Transactions on Antennas and Propagation*, 29 (1), pp. 2-24 (1981), https://doi.org/10.1109/TAP.1981.1142523.

[32] T. A. Miligan, "Modern Antenna Design" (John Wiley and Sons Ltd., Hoboken, New Jersey, USA, 2005, 2nd edn.), pp. 293–319.

[33] D. M. Pozar, "Microstrip antennas," *Proceedings of the IEEE*, 80 (1), pp. 79-91 (1992).

[34] R. Bancroft, "Microstrip and Printed Antenna Design" (SciTech Publishing Inc., Raleigh, NC, USA, 2009,2nd edn.), pp. 142–176.

[35] R. P. Owens, "Microstrip antenna feeds," in James, J. R., Hall, P. S. (Ed.): "Handbook of Microstrip Antennas" (Peter peregrines Ltd., London, UK, 1989, 1st edn.), pp. 815–855.

[36] "Link budget calculations," https://www.kymetacorp.com/wp-content/uploads/2019/06/Link-Budget-Calculations-2.pdf, accessed March 2021.

[37] "Calculations for Space Communication," http://propagation.ece.gatech.edu/ECE6390/project/Sum2015/team5/satellite-downlink.html, accessed April 2021.

[38] D. Roddy, "Satellite Communications" (McGraw-Hill Companies, Inc., New York, NY, USA, 2006, 4th edn.), pp.351–368.